Viscous fingering of a draining suspension

Yun Chen,[1] Frank Malambri,[2] and Sungyon Lee[1,*]
[1]*Department of Mechanical Engineering, University of Minnesota, Minneapolis, Minnesota 55455, USA*
[2]*Department of Aerospace Engineering, Texas A&M University, College Station, Texas 77843, USA*

(Received 20 June 2017; published 24 September 2018)

The liquid drainage is a commonplace process that affects a wide array of industrial applications ranging from medical procedures and manufacturing processes to food processing. While many drainage-related applications involve the complex fluids comprising solid particles, the effects of suspended particles on the liquid drainage have not been considered, leaving simple fundamental questions on the suspension drainage unanswered. In this paper, we experimentally investigate the effects of particles on drainage by withdrawing suspensions from an air-filled Hele-Shaw cell in a radial sink flow. As expected, viscous fingering arises as air invades a draining viscous suspension. Despite numerous studies on viscous fingering, only a few have studied this "inward" viscous fingering for pure liquids and none for suspensions. We find that, while the overall behavior of fingering remains unchanged from the pure liquid case, suspended particles are shown to delay the onset of fingering but also to accelerate its growth rate. This surprising dual effect of particles results in the increase of the total drainage time and in the amount of drained suspension as a function of particle concentrations. In addition, the particle entrainment into the thin film of wetting oil causes particles with select sizes to remain on the channel walls instead of draining, which closely follows our simple theoretical prediction.

DOI: 10.1103/PhysRevFluids.3.094001

I. INTRODUCTION

Draining is a commonplace process that is present in all aspects of life. It can be as innocuous as water draining down a sink or can have serious medical implications in the case of draining excess fluid from the chest cavity [1,2] to treat pleural effusion [3,4]. Efficient and complete drainage also affects a plethora of industrial applications that range from plant biotechnology techniques [5] and biomedical manufacturing [6,7] to food processing. For instance, cleaning food production lines requires the complete drainage of various food items which are often emulsions or suspensions [8,9]. The drainage of suspensions is also found in the inkjet-based direct writing of biological cells [10]. Here, the bioink suspension is ejected from a chamber and deposited onto the substrate [11,12]; other types of bioink for 3D printing may include mammalian cells [7] or bacteria [6]. Hence many of the relevant applications of today involve the drainage of complex fluids, or suspensions.

Despite the ubiquity and diversity of problems that are associated with draining, fundamental fluid mechanics research on drainage remains relatively limited. Progress has been made in three distinct types of draining flows: liquid drainage from a tank through a small orifice [13–15], dip coating of viscous fluid [16–20], and oil drainage from a confined 2D channel [21]. Despite their differences, the focus of all three studies lies in the dynamics of the evolving fluid-fluid interface, whether it is the deformation of the receding free surface [13–15,21] or the deposition of the thin film on the solid surface upon liquid withdrawal [16–20].

*sungyon@umn.edu

In this paper, we focus on the drainage of viscous liquid from an air-filled 2D channel, in which a less wetting and less viscous fluid (air) displaces a more viscous fluid that preferentially wets the channel. Under this circumstance, the fluid-fluid interface is unstable and leads to the onset of viscous fingering during drainage [22]. In particular, Paterson [21] experimentally observed that when the oil withdraws from air in a radial sink flow, the oil-air interface becomes unstable and starts fingering towards the center hole. The analogous fingering behavior was also investigated theoretically by calculating the interfacial shapes of a 2D circular drop subject to suction [23–27]. The most striking observation here is the direct coupling between the fingering dynamics and drainage stoppage: the oil drainage comes to a halt when the fastest growing finger reaches the center orifice. Hence the evolution of the receding interface is the key factor in determining the complete versus incomplete drainage of given fluid, which can affect the host of drainage-related applications. However, compared to extensive works on viscous fingering both in rectilinear and radial source flows [21,28–31], the study of "inward" viscous fingering remains sparse even for pure liquids and nonexistent for more complex fluids, such as suspensions.

Given the prevalence of suspensions in draining processes and the coupled dynamics of fingering and drainage, we presently consider the viscous fingering of a draining suspension and its effect on draining efficiency. Despite the identical setup, our work is distinct from that of Paterson [21], due to the complex particle dynamics especially near the draining interface. A recirculation flow near the interface renders the particle migration inherently three dimensional, which invalidates the use of depth-averaged theoretical tools (i.e., Darcy's law) in our present problem. The importance of 3D effects in fingering phenomena was previously demonstrated in miscible fingering in porous media [32–37], as well as in setting the onset of miscible fingering in a Hele-Shaw cell [38–41]. Specifically, we experimentally test the effects of neutrally buoyant particles on the dynamics of the fastest growing finger that directly controls the total amount of drained oil, as suspensions withdraw from a Hele-Shaw cell. The present study also adds to a growing body of work that demonstrates the effects of suspended particles on interfacial dynamics. The previous work in this topic includes the pinch-off of a suspension droplet [42–47], free-surface, particle-laden flows down an incline [48–56], particle-induced viscous fingering [57–60], and emergence of various interfacial patterns upon the injection of air into a suspension [61–65].

The experimental results in Sec. III reveal that the finger grows faster with particle concentrations ϕ_0, while the total drainage time and the amount of oil drainage also increase with ϕ_0. These contradictory results allude to the dual effects of suspended particles to delay and to accelerate fingering. In addition, particles of select sizes are observed to coat the channel surfaces and not drain, reminiscent of colloidal assembly in dip coating [66]. The summary and future work are included in Sec. IV.

II. EXPERIMENTAL SETUP

We conduct the suspension drainage experiments in a Hele-Shaw cell that consists of two parallel plexiglass plates ($30.5 \times 30.5 \times 3.8$ cm). The plates are separated by a gap thickness $h = 1.39 \pm 0.015$ mm; the bottom plate has a small hole drilled in the center through which the suspension is drained [Fig. 1(a)]. The suspension of the particle volume fraction, ϕ_0, is prepared by mixing neutrally buoyant polyethylene particles (density $\rho_p = 1.00$ g/cm^3, diameter $d = 130 \pm 15$ μm; Cospheric) with a PMMS silicone oil (density $\rho_l = 0.96 \pm 0.01$ g/cm^3 and dynamic viscosity $\eta_l = 0.096 \pm 0.01$ Pa s) in a syringe. The value of ϕ_0 is varied between 0.05 and 0.2 with an increment of 0.01.

We first inject the suspension into the Hele-Shaw cell to the radius of $R_0 \approx 10$ cm [Fig. 1(b)]. Notably, the maximum value of ϕ_0 is set at 0.2 to prevent the inhomogeneous distribution of particles and miscible fingering upon initial injection, as previously observed by Xu and colleagues [59]. The suspension is then withdrawn from the center at a fixed flow rate Q (i.e., $Q = 4.5 \pm 0.25,\ 5.7 \pm 0.15,\ 6.1 \pm 0.2,\ 6.8 \pm 0.35$, and 9.2 ± 0.4 ml/min). A high resolution camera (1920×1080 pixel images, FOV 60°) records the suspension drainage experiments from directly

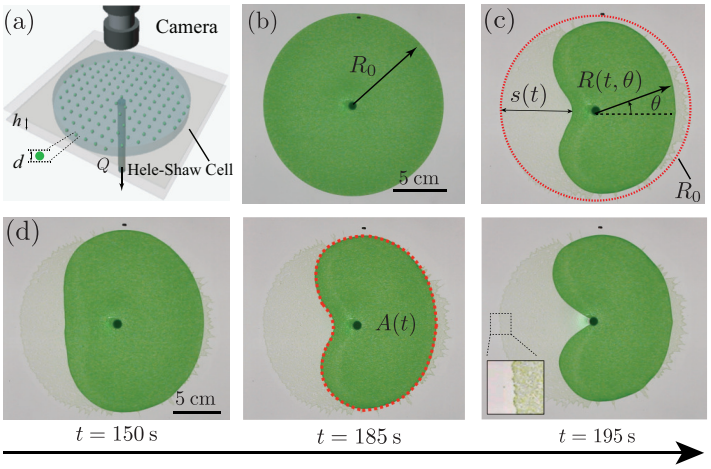

FIG. 1. (a) Schematic of the experimental setup: suspensions are drained through the center of the Hele-Shaw cell. Time-elapsed images are taken by the camera placed directly above. (b) Initial circular shape of the suspension with $\phi_0 = 0.1$ and radius $R_0 \approx 10$ cm. (c) $R(t, \theta)$ is defined as the distance from the center to each point of the interface at given time, t, while s is the distance between the finger tip $R_{\min}$ and R_0, or $s(t) = R_0 - R_{\min}(t)$. (d) Time-evolution images of a $\phi_0 = 0.1$ suspension that is drained at $Q = 6.8$ ml/min. A finger initiates after $t = 150$ s and grows until it reaches the center. $A(t)$ is defined as the instantaneous area of the draining suspension.

above the Hele-Shaw cell. The instantaneous radius $R(t, \theta)$ corresponds to the distance from the center to each point on the interface at an angle θ and is obtained using MATLAB image processing tools [Fig. 1(c)]. We also extract the instantaneous area of the draining suspension $A(t)$ based on $A(t) = (1/2)\int_0^{2\pi} R^2(t, \theta)d\theta$ [Fig. 1(d)] and its time rate of change $\dot{A}(t)$. For given Q, $\dot{A}(t)$ is approximately constant in time but surprisingly varies with ϕ_0, which will be addressed later in the text. We hereby define $\bar{q}$ that corresponds to the value of $|\dot{A}(t)|$ averaged over ϕ_0 for given Q, so that the characteristic time scale of the draining suspension is given by $\bar{t} \equiv \pi R_0^2/\bar{q}$.

III. RESULTS

Various physical phenomena emerge when a suspension, instead of pure oil, drains from air in a radial sink flow. For instance, as evident in the images in Fig. 1(d), some particles are left behind on the plates and provide pinning sites for the retracting air-suspension interface, which can lead to complex interfacial morphologies. In some cases, particle accumulation or depletion is observed near the retracting interface. Despite such added complexities, the most critical aspect of inward fingering experiments [21,67] appears intact: the drainage of suspension stops when the finger reaches the center hole, which is the focus of our present work. To ensure that the interfacial shape is not determined by pinning, we only consider experimental data in which no pinning of the retracting interface is observed during drainage.

Notably, only one finger emerges during the entire drainage process in our experiments, which may be due to the range of the capillary number $\mathrm{Ca} \sim O(10^{-3})$, as well as the size of perturbations that are inherent to our current setup. Here, $\mathrm{Ca} \equiv \eta(\phi_0)\bar{q}/(\gamma 2\pi R_0)$, where $\eta(\phi_0)$ corresponds to the effective viscosity of a suspension, while γ is surface tension. Note that $\eta(\phi_0)$ is replaced with η_1 when we refer to Ca from previous studies with pure liquids. Previously, multiple inward fingers were observed when a viscous fluid drains from a less viscous fluid [21,67], but these studies were conducted at moderate values of Ca. The inward viscous fingering in the multifinger regime [$\mathrm{Ca} \sim O(10^{-1})$] was also numerically considered by Chen and colleagues [27]. The range of Ca in the present study is consistent with the numerical simulations by Kelly and Hinch [23] who

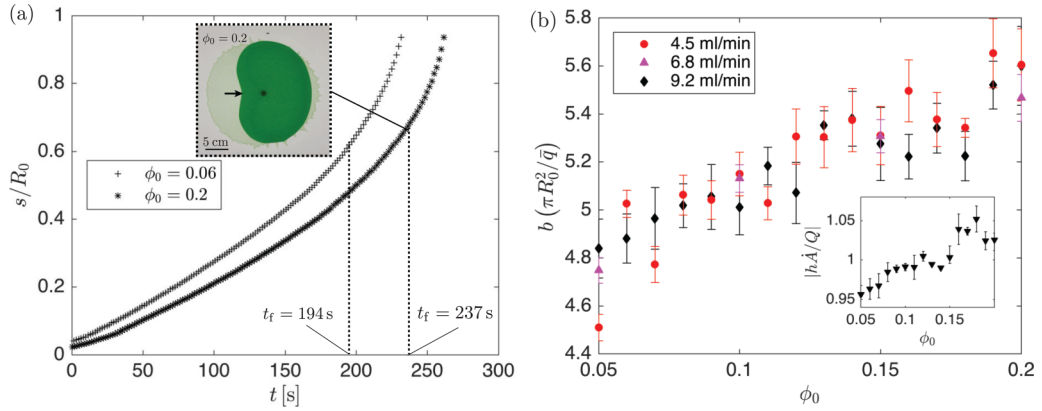

FIG. 2. (a) Time evolution of dimensionless deviation, s/R_0, for two different initial particle concentrations, $\phi_0 = 0.06$ and 0.2, with $Q = 4.5$ ml/min. The inset image of the suspension for $\phi_0 = 0.2$ with $Q = 4.5$ ml/min shows an example of fingering onset at $t_f = 237$ s. (b) The fingering growth rate, b, is extracted by fitting the $s - t$ curve with the exponential function, $s \propto \exp(bt)$, for $t > t_f$; the resultant b is then normalized by $\pi R_0^2/\bar{q}$ and plotted as a function of ϕ_0. The inset plot shows that the dimensionless speed of the retracting interface, $|h\dot{A}/Q|$, increases with ϕ_0.

observed one inward finger in a similar flow configuration. However, it is important to acknowledge that the current fingering mode could also be influenced by the perturbations in our system, as the experiments appear sensitive to the actual setup (see the next paragraph). Despite uncertainty in its origin, the emergence of a single finger is a uniquely simple limit of an inward fingering problem. We will presently take advantage of this simplicity and focus on the onset and growth of a single finger only in this study.

In Fig. 1(d), the time-evolution images of the suspension of $\phi_0 = 0.1$ illustrate the typical suspension drainage experiment set at $Q = 6.8$ ml/min. From the start of drainage (i.e., $t = 0$ s), the suspension-air interface starts retracting towards the center; the interface moves asymmetrically as the displacement of a viscous liquid by air is inherently unstable [21,28,31]. In our experiments, the location of incipient symmetry breaking and fingering is observed to strongly depend on the inherent imperfections (i.e., slight unevenness) of the plates. This is evidenced by the fact that the fingering location changes when the plates are rotated. Hence, to keep the conditions between the experiments consistent, we have used the identical plate configuration for all the experiments reported here, which somewhat artificially fixes the location of symmetry breaking as a result. Going back to Fig. 1(d), the interface becomes flat on one side at $t = 150$ s and starts to finger inwardly. Accordingly, the onset of a viscous finger is defined as the moment of transition in the interfacial shape from convex to concave and is given by $t_f = 165$ s. Upon its formation at $t = t_f$, the finger continues to grow towards the center and the drainage ceases once the fingertip reaches the center at $t_c = 195$ s. Hence the dynamics of the finger must directly determine the total amount of drained suspension.

A. Finger growth speed

The evolution of the growing finger is quantified by extracting the deviation of the minimum distance to the interface $R_{\min}(t)$ from the initial radius R_0, such that $s(t) = R_0 - R_{\min}(t)$. In Fig. 2(a), the plot of s versus t at $Q = 4.5$ ml/min shows that the draining stops, or $s(t)/R_0 \to 1$, at an earlier time for $\phi_0 = 0.06$ than for $\phi_0 = 0.2$. However, it is difficult to determine the fingering growth rate from this $s - t$ curve directly since the finger does not occur from the beginning of each experiment. Therefore, we first extract the time of the fingering onset t_f from each experiment; the inset image of Fig. 2(a), for instance, shows that the finger forms at $t_f = 237$ s for $\phi_0 = 0.2$ and

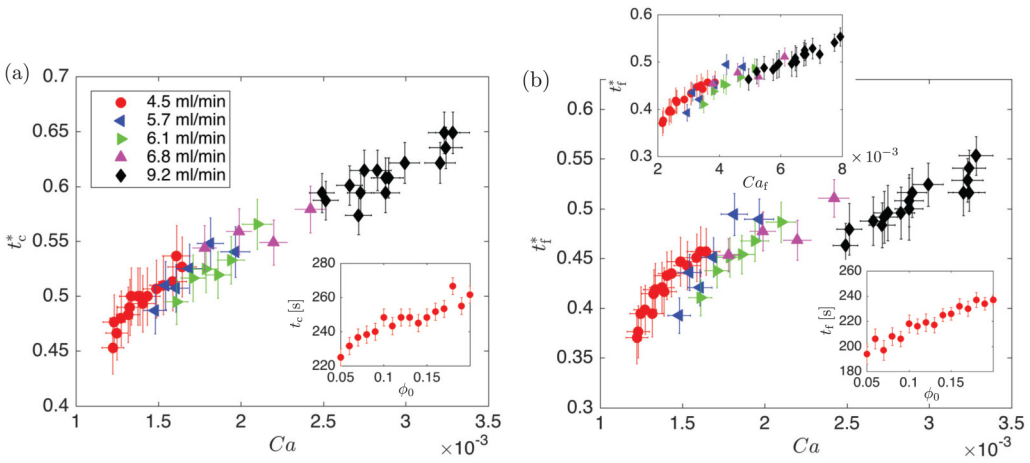

FIG. 3. (a) Dimensionless time of completion of drainage, $t_c^* = t_c\bar{q}/(\pi R_0^2)$, increases with the effective capillary number, Ca $\equiv \eta(\phi_0)\bar{q}/(\gamma 2\pi R_0)$. Notably, t_c^* is analogous to the dimensionless volume of the drained suspension. The inset figure shows that dimensional t_c increases with ϕ_0 for $Q = 4.5$ ml/min. (b) The dimensionless time of fingering onset, $t_f^* = t_f\bar{q}/(\pi R_0^2)$, also increases with Ca; the top left inset shows the considerably improved collapse in t_f^* as a function of modified capillary number, $\mathrm{Ca_f}$; the corresponding dimensional plot of t_f versus ϕ_0 is included in the bottom right inset for $Q = 4.5$ ml/min.

$Q = 4.5$ ml/min. Then, the dimensional growth rate b is obtained by empirically fitting the $s - t$ curve to the exponential function, $s \propto \exp(bt)$, only for $t > t_f$.

The resultant value of b is normalized by $\bar{q}/(\pi R_0^2)$ and is plotted as a function ϕ_0 in Fig. 2(b). At given Q, b increases with ϕ_0, which can be rationalized by considering the effect of suspended particles on the overall viscosity, $\eta(\phi_0)$. Here, $\eta(\phi_0)$ is given by $\eta(\phi_0)/\eta_l = 1 + 2.5\phi_m^2(\phi_m - \phi_0)^{-1} + 0.1\phi_0^2(\phi_m - \phi_0)^{-2}$ [68], where $\phi_m \approx 0.62$ is the maximum packing fraction. An increase in ϕ_0 corresponds to a higher viscosity difference between the suspension and air, or $\eta(\phi_0) - \eta_{air}$, and must lead to a faster growing finger. Hence the increase of b with ϕ_0 and, by extension, $\eta(\phi_0)$ qualitatively agrees with the numerical simulations of Kelly and Hinch [23] who found the fingertip velocity to increase with the capillary number in the case of a draining liquid. Notably, Kelly and Hinch [23] introduced an initial offset between the center of liquid and the point of drainage, which differs from our initial condition. However, they found that the finger geometry and speed are insensitive to the offset, which helps justify the qualitative comparison between our current experiments and their simulation results.

B. Total time of drainage completion

From the standpoint of drainage efficiency in various applications, the most important result to consider is the total time of drainage t_c, which directly corresponds to the total volume of the recovered suspension, or $V_t = Qt_c$. Surprisingly, despite the increase in the fingertip speed with ϕ_0, t_c also increases with ϕ_0, as clearly shown in the inset of Fig. 3(a) for $Q = 4.5$ ml/min. This is also evident in the $s - t$ curve in Fig. 2(a). The counterintuitive correlation between the fingertip speed and the drainage time demonstrates that the onset of finger formation must be delayed with increasing ϕ_0. Accordingly, the time of fingering onset t_f is shown to increase with ϕ_0 in the bottom right inset of Fig. 3(b).

This delay in the fingering onset cannot be explained by simply considering the effect of particles on the effective viscosity alone. In the pure liquid counterpart, fingering is expedited when the viscosity ratio between the invading and defending fluids is increased [40,41]. This is in direct contrast with the behavior of a draining suspension, in which the increase in $\eta(\phi_0)$ increases the

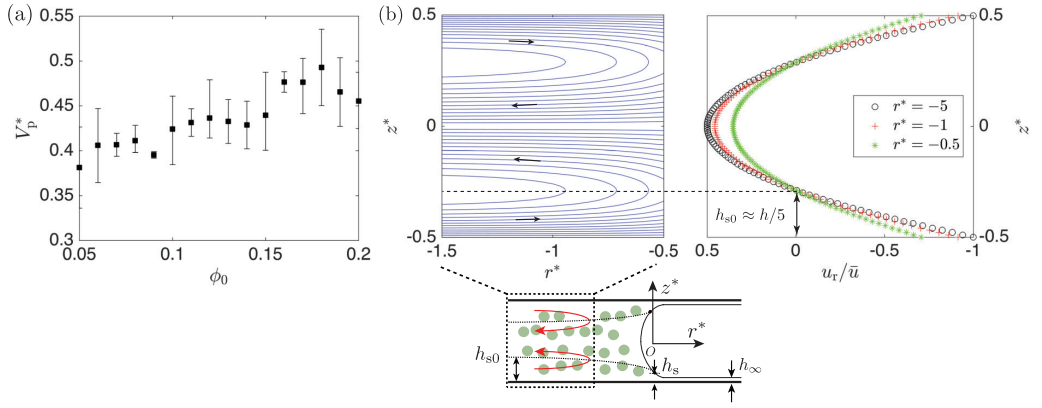

FIG. 4. (a) Normalized total volume of suspension left on the plate, V_p^*, increases with ϕ_0 at $h = 1.39$ mm, Q. (b) Bottom: the schematics of the side view of suspension in the Hele-Shaw cell. There exists a recirculation flow near the interface, where h_{s0} is the point of flow reversal and connects to the stagnation point on the meniscus, h_s. Here, h_∞ is the thin flim coating the plate. Top left: the plot of streamlines of the fountain flow near the interface based on the simplified analytic solution. Top right: normalized radial velocity, $u_r/\bar{u}$, is plotted as a function of z^* at various values of r^* from the interface. The distance from the wall at which $u_r = 0$ is computed to be $h_{s0} \approx h/5$.

viscosity ratio between the suspension and invading air but clearly delays the onset of fingering. Further studies are required to elucidate the complex role of suspended particles to delay the start but to accelerate the inward fingering once it is formed.

The results for varying ϕ_0 and flow rates are summarized in the plot of the dimensionless completion and onset times, $t_c^* = t_c/\bar{t}$ and $t_f^* = t_f/\bar{t}$, where $\bar{t} = \pi R_0^2/\bar{q}$, as a function of Ca in Fig. 3. While t_c^* exhibits a reasonable collapse across all flow rates, the plot of t_f^* versus Ca suggests that t_f^* may increase linearly with the capillary number but with the slope that varies with the flow rate. Interestingly, the collapse in t_f^* is shown to improve considerably when it is plotted as a function of the modified capillary number, $\mathrm{Ca_f} = \eta(\phi_0)\bar{q}/[\gamma 2\pi R_f(\phi_0)]$, in the top left inset of Fig. 3(b); no significant change is noted for t_c^* and is hence not reproduced. Here, $R_f = R_{\min}(t_f)$, or the distance between the fingertip and the injection hole at the onset of fingering [see the inset image of Fig. 2(a)]. Hence $\mathrm{Ca_f}$ incorporates both the effects of particles in modifying the effective viscosity [i.e., $\eta(\phi_0)$] as well as in setting the fingering onset [i.e., $R_f(\phi_0)$]. While the choice of $\mathrm{Ca_f}$ is somewhat *ad hoc* and lacks the physical insight, this further illustrates one key fact: the effect of particles in modifying the viscosity alone does not sufficiently capture the full complexity of the current experiments.

C. Particle drainage versus entrainment

Another unexpected result is found in the dimensionless speed of the retracting interface, $|h\dot{A}/Q|$, that *increases* with ϕ_0, as shown in the inset of Fig. 2(b). To explain this, we must consider how the suspension area $A(t)$ is coupled to the amount of suspension that is left behind on the plate surfaces V_p, or $A(t) = A(t=0) - [Qt + V_p(t)]/h$. Hence, at given Q, the increase in $|\dot{A}|$ with ϕ_0 must result in the greater final volume of suspension left on the surface $V_p(t_c)$, as confirmed by the plot of $V_p^*(t_c) = V_p(t_c)/(t_c Q)$ as a function of ϕ_0 in Fig. 4(a).

Then what causes some particles to be left behind on the plates, instead of draining into the sink? As the air-suspension interface retracts towards the center hole, there exists a recirculation flow near the interface as shown in the schematics in Fig. 4(b). Particles are entrained into thin films of oil (thickness h_∞) coating the plates owing to this recirculation flow and remain on the plate surfaces. Here, $r^* = r/h$ and $z^* = z/h$ are the dimensionless coordinates with the origin at the center of the interface. Particle entrainment into thin films of viscous liquid has been previously studied in the

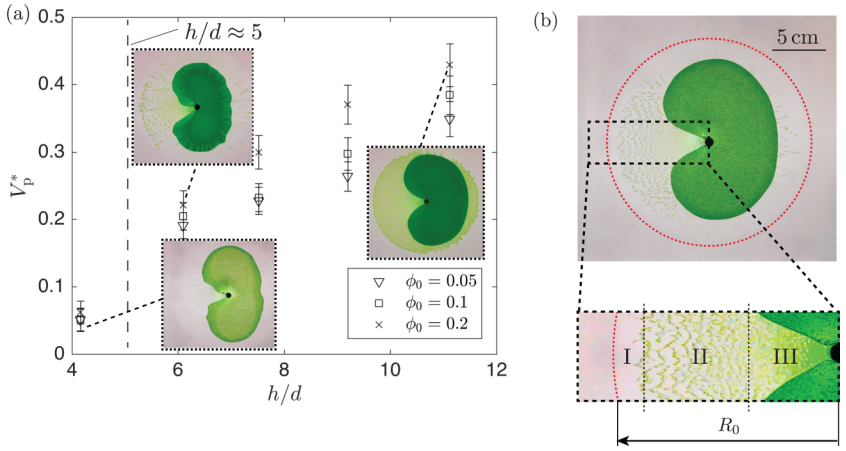

FIG. 5. (a) Plot of V_p^* versus h/d for $\phi_0 = 0.05$, 0.1, and 0.2 shows that V_p^* strongly depends on the channel gap thickness, h, relative to the particle diameter, d, at $Q = 6.8$ ml/min. (b) A snapshot shows different patterns of particle deposition upon the draining completion for $Q = 6.8$ ml/min and $h = 0.94$ mm. In region I, no particles deposited on the plate. In region II, the striped pattern of particles is observed, while in region III this periodic pattern transits to uniform deposition. Here, R_0 is the initial radius of the interface.

context of dip coating of colloidal suspensions [66,69–72]. In particular, Colosqui and colleagues [66] found that, as the plate is pulled from the bath of suspensions, particles entrain into the thin film only when they are small enough to fit inside the shear flow region near the plate. In this line of thought, the criterion of the particle entrainment in the present experiments is $d < h_s$, where h_s is the stagnation point on the meniscus that separates the local shear flow from the bulk flow [66] [see the schematic in Fig. 4(b)].

Computing h_s involves resolving the local interfacial speed and shape of the meniscus coupled to the film thickness h_∞, which can be quite challenging. However, one can obtain a reasonable estimate for h_s by considering the simplified recirculation flow near the meniscus, also known as the "fountain flow" [73]. The stream function ψ for the fountain flow [74] corresponds to

$$\psi = -\frac{Qz^*}{4\pi}(1 - 4z^{*2})[1 - \exp(r^*\sqrt{6})]. \tag{1}$$

Note that ψ neglects the effect of particles on the flow itself and does not account for the shape of the evolving meniscus and the film thickness h_∞. Despite its limitations, Eq. (1) qualitatively captures key flow characteristics for $|r^*| > 0.5$, or the boxed region in the schematic of Fig. 4(b). The corresponding streamlines within the range $-1.5 < r^* < -0.5$ on the top left of Fig. 4(b) reveal the flow reversal near the wall that may redirect particles towards the meniscus. To further quantify this reverse flow, the dimensionless radial component of velocity, $u_r/\bar{u}$, is computed based on $u_r = -(1/r)(\partial\psi/\partial z)$, where $\bar{u}$ is the mean velocity of the interface. As shown in the top right of Fig. 4(b), the distance from the wall h_{s0} at which $u_r = 0$ corresponds to $h/5$ and separates the back flow towards the meniscus (i.e., $u_r/\bar{u} < 0$) from the draining flow (i.e., $u_r/\bar{u} > 0$). As h_{s0} eventually connects to the stagnation point on the meniscus, it works as a reasonable estimate for h_s. Hence particles whose diameter d is less than h_{s0} are likely to be trapped in the meniscus and entrained into thin wetting films on the plates.

Consistent with this leading order entrainment criterion of $d < h_{s0} \approx h/5$, the value of V_p^* plotted in Fig. 5(a) exhibits a steep drop from $O(10^{-1})$ to $O(10^{-2})$ when h/d is lowered from 6 to 4, independent of ϕ_0. Here, the value of h/d is varied by modulating h (i.e., $h = 0.52, 0.76, 0.94, 1.15, 1.39$ mm), while the particle diameter d remains fixed at 130 μm. For $h/d > 5$, the value of V_p^* is shown to diverge with varying ϕ_0 in Fig. 5(a). In addition to the V_p^*

dependency on ϕ_0, we also observe different patterns of particles that are left behind the retracting interface (see the images in Fig. 5). While the quantitative analysis is beyond the scope of the present study, we hereby qualitatively describe and rationalize this nonuniform distribution of particles on the plates based on the scaling argument.

According to the seminal works on the dynamics of thin coating flows [16,66,75,76], h_s/h must scale with $\mathrm{Ca}_i^{2/3}$, where $\mathrm{Ca}_i \equiv \mu U_i/\gamma$ and U_i is the time-dependent speed of the retracting interface, not the average value that was previously used. This time-dependent nature of h_s leads to the time-dependent particle deposition and hence nonuniform distribution of particles on the plates, as illustrated in Fig. 5(b). For instance, even when $h/d > 5$ (leading order criterion for entrainment), no particles may be deposited onto the plates initially if $d > h_s \sim h\mathrm{Ca}_i^{2/3}$, as evident in region I of Fig. 5(b) with $h/d \approx 7$. As h_s increases close to d with increasing U_i, particles become entrained into the thin coating film of oil in "chunks," in agreement with the simulations of multiparticle interactions [66] when d is slightly greater than h_s. This physical picture is consistent with the striped pattern of particles that are deposited on the plates in Fig. 5(b), region II. When $d < h_s$ with the further increase in U_i, the periodic particle deposition transitions to uniform deposition, as observed in region III of Fig. 5(b). Alternatively, even when $h/d < 5$ (no particle entrainment), we often observe a small amount of particles that are left on the plates very close to the injection hole where U_i and hence h_s are the largest.

IV. DISCUSSION

In summary, we experimentally investigate the effect of neutrally buoyant particles on the interfacial dynamics of a draining suspension and its influence on drainage efficiency, which are relevant in various biotechnology and manufacturing processes. Our results show that the finger grows and reaches the sink faster with higher ϕ_0 that corresponds to an increase in the effective capillary number Ca. This result qualitatively agrees with the numerical simulations by Kelly and Hinch [23], who predicted a faster finger growth rate with Ca for a draining fluid. Despite the increase in the fingertip speed, we find that the total time of drainage and the total volume of drained suspension also increase when more particles are added. Hence the addition of particles can potentially enhance the drainage efficiency of the suspension. However, the quantitative relationship between the number of fingers and Ca as well as the finger geometry have not yet been established. For instance, the wavelength of the maximum growth rate currently does not match the theoretical prediction by Paterson [21]. Similarly, Chevalier *et al.* [63], who injected air into a dilute suspension, found the finger width to be larger than liquid with the equivalent viscosity for $h/d \lesssim 10$. Currently, no explanation is available to rationalize this deviation between the suspension and the pure liquid counterpart and warrants further systematic investigation. One conjecture is that the nontrivial particle dynamics normal to the plates must render our current system three dimensional, distinct from the mostly 2D nature of immiscible fingering in a Hele-Shaw cell.

In addition, particle entrainment into the thin film of oil causes some particles not to drain but to remain on the plates. This gives rise to nonzero V_p^*, or the volume of suspension left on the plates. Based on an analytic solution of the "fountain flow" downstream of the retracting interface [73,74], we derive the particle entrainment criterion to be $h/d > 5$, which closely matches the experimental results. In turn, the amount of V_p^* directly influences the speed of the retracting interface, as $|h\dot{A}/Q|$ is found to increase with V_p^* and, thereby, ϕ_0. Furthermore, for $h/d > 5$, we observe that particles are deposited onto the substrates in a nonuniform fashion. We qualitatively rationalize this observation by considering the stagnation point on the meniscus that increases with the time-dependent speed of the retracting interface.

Overall, understanding the effects of suspended particles on fluid-fluid interfaces applies to diverse engineering processes that go beyond the aforementioned applications. In particular, aspects of the current research (i.e., particle entrainment) are directly relevant to the dip coating with suspensions [66,69–72], evaporation of complex drops, such as blood, [77] that yield coffee-ring

effects [78], and even nanoparticle printing [79,80]. However, despite the growing interest in the interfacial dynamics of suspensions, many unanswered questions persist and the continuum level description of suspensions appears to fall short. For instance, the counterintuitive correlation between the drainage time and fingertip speed in the present study indicates that the onset of fingering must be delayed with increasing ϕ_0. The delay in fingering onset cannot be explained with the increasing effective viscosity ratio between the suspension and air alone [i.e., $\eta(\phi_0)/\eta_{\text{air}}$], as fingering initiates sooner with the increasing viscosity ratio in the pure liquid case [40,41]. The effect of particles to delay the onset of fingering yet to accelerate it upon formation may require the grain-scale understanding of the suspensions and remains the topic of future investigation. Lastly, our present study takes an initial step towards quantifying the effect of noncolloidal particles on the formation and dynamics of a single finger. The future work requires considering a wider parameter space (i.e., particle sizes, channel geometry, and capillary numbers) to investigate the effect of particles on multiple fingers, which is of interest in many biotechnology and industrial applications.

ACKNOWLEDGMENTS

The authors wish to thank Dr. Jungchul Kim for fruitful discussions and Dr. Irmgard Bischofberger (MIT) for her helpful feedback on the manuscript. The financial support for this work was provided by the Texas A&M Engineering Experiment Station (TEES). F.M. acknowledges an Undergraduate Summer Research Grant at Texas A and M University for funding.

[1] H. West, Malignant pleural effusion, JAMA Oncol. **1**, 260 (2015).
[2] C. Zisis, K. Tsirgogianni, G. Lazardis, S. Lampaki, S. Baka, I. Mpoulovinas, V. Karavasilis, I. Kioumis, G. Pitsiou, N. Katsikogiannis, K. Tsakiridis, A. Rapti, G. Trakada, I. Karapantzos, C. Karapantzou, A. Zissimopoulos, K. Zarogoulidis, and P. Zarogoulidis, Chest drainage system in use, Ann. Transl. Med. **3**, 43 (2015).
[3] S. McDermott, D. A. Levis, and R. S. Arellano, Chest drainage, Semin. Intervent. Rad. **29**, 247 (2012).
[4] R. Light, *Pleural Diseases* (Lippincott Williams & Wilkins, Philadelphia, 2013), Chap. 3.
[5] M. Raviv and J. H. Lieth, *Soilless Culture: Theory and Practice* (Elsevier Science, Amsterdam, 2008), Chap. 5.
[6] T. Xu, S. Petridou, E. H. Lee, E. A. Roth, N. R. Vyavahare, J. J. Hickman, and T. Boland, Construction of high-density bacterial colony arrays and patterns by the ink-jet method, Biotechnol. Bioeng. **85**, 29 (2004).
[7] T. Xu, Y. Jin, C. Grefory, J. J. Hickman, and T. Boland, Inkjet printing of viable mamalian cells, Biomaterials **26**, 93 (2005).
[8] J. E. Taylor, I. van Damme, M. L. Johns, A. F. Routh, and D. I. Wilson, Shear rheology of molten crumb chocolate, J. Food Sci. **74**, E55 (2009).
[9] A. Ali, A. Underwood, Y. R. Lee, and D. I. Wilson, Self-drainage of viscous liquids in vertical and inclined pipes, Food Bioprod. Process **99**, 38 (2016).
[10] B. R. Reingeisen, C. M. Othon, J. A. Barron, D. Young, and B. J. Spargo, Jet-based methods to print living cells, Biotechnol. J. **1**, 930 (2006).
[11] M. Nakamura, A. Kobayashi, F. Takagi, A. Watanabe, Y. Hiruma, K. Ohuchi, Y. Iwasaki, M. Horie, I. Morita, and S. Takatani, Biocompatible inkjet printing technique for designed seeding of individual living cells, Tissue Eng. **11**, 1658 (2005).
[12] S. Khalil, J. Nam, and W. Sun, Multi-nozzle deposition for construction of 3d biopolymer tissue scaffolds, Rapid Prototyping J. **11**, 9 (2005).
[13] B. T. Lubin and G. S. Springer, The formation of a dip on the surface of a liquid draining from a tank, J. Fluid Mech. **29**, 385 (1967).

[14] Q. N. Zhou and W. P. Graebel, Axisymmetric draining of a cylindrical tank with a free surface, J. Fluid Mech. **221**, 511 (1990).
[15] Q. N. Zhou and W. P. Graebel, Free-surface oscillations in a slowly draining tank, J. Appl. Mech. **59**, 438 (1992).
[16] L. D. Landau and B. G. Levich, Dragging of a liquid by a moving plate, Acta Physicochim. U.R.S.S. **17**, 42 (1942).
[17] K. J. Ruschak, Coating flows, Annu. Rev. Fluid Mech. **17**, 65 (1985).
[18] L. E. Scriven, Physics and applications of dip coating and spin coating, MRS Proc. **121**, 717 (1988).
[19] P. R. Schunk, A. J. Hurd, and C. J. Brinker, Free-meniscus coating processes, in *Liquid Film Coating: Scientific Principles and Their Technological Implications*, edited by S. F. Kistler and P. M. Schweizer (Springer Netherlands, Dordrecht, 1997), pp. 673–708.
[20] D. Quere, Fluid coating on a fiber, Annu. Rev. Fluid Mech. **31**, 347 (1999).
[21] L. Paterson, Radial fingering in a Hele Shaw cell, J. Fluid Mech. **113**, 513 (1981).
[22] J. Ortn and S. Santucci, Avalanches, non-Gaussian fluctuations and intermittency in fluid imbibition, in *Avalanches in Functional Materials and Geophysics*, edited by E. K. H. Salje, A. Saxena, and A. Planes (Springer, New York, 2017), pp. 261–292.
[23] E. D. Kelly and E. J. Hinch, Numerical simulations of sink flow in the Hele-Shaw cell with small surface tension, Eur. J. Appl. Math. **8**, 533 (1997).
[24] H. D. Ceniceros, T. Y. Hou, and H. Si, Numerical study of Hele-Shaw flow with suction, Phys. Fluids **11**, 2471 (1999).
[25] C. Y. Chen, C. W. Huang, H. Gadelha, and J. A. Miranda, Radial viscous fingering in miscible Hele-Shaw flows: A numerical study, Phys. Rev. E **78**, 016306 (2008).
[26] C. Y. Chen, Y. S. Huang, and J. A. Miranda, Diffuse-interface approach to rotating Hele-Shaw flows, Phys. Rev. E **84**, 046302 (2011).
[27] C. Y. Chen, Y. S. Huang, and J. A. Miranda, Radial Hele-Shaw flow with suction: Fully nonlinear pattern formation, Phys. Rev. E **89**, 053006 (2014).
[28] P. G. Saffman and G. I. Taylor, The penetration of a fluid into a porous medium or Hele-Shaw cell containing a more viscous liquid, Proc. R. Soc. London A **245**, 312 (1958).
[29] R. L. Chuoke, P. van Meurs, and C. van der Poel, The instability of slow, immiscible, viscous liquid-liquid displacements in permeable media, J. Petrol. Technol. **11**, 64 (1959).
[30] P. G. Saffman, Viscous fingering in a Hele-Shaw cell, J. Fluid Mech. **173**, 73 (1986).
[31] G. M. Homsy, Viscous fingering in porous media, Annu. Rev. Fluid Mech. **19**, 271 (1987).
[32] J.-C. Bacri, D. Salin, and R. Woumeni, Three-Dimensional Miscible Viscous Fingering in Porous Media, Phys. Rev. Lett. **67**, 2005 (1991).
[33] W. B. Zimmerman and G. M. Homsy, Three-dimensional viscous fingering: A numerical study, Phys. Fluids **4**, 1901 (1992).
[34] M. A. Christie, A.H. Muggeridge, and J. J. Barley, 3d simulation of viscous fingering and wag schemes, SPE Reservior Eng. **8**, 19 (1993).
[35] A. Riaz and E. Meiburg, Three-dimensional miscible displacement simulations in homogeneous porous media with gravity override, J. Fluid Mech. **494**, 95 (2003).
[36] A. De Wit, Y. Bertho, and M. Martin, Viscous fingering of miscible slices, Phys. Fluids **17**, 054114 (2005).
[37] T. Suekane, J. Ono, A. Hyodo, and Y. Nagatsu, Three-dimensional viscous fingering of miscible fluids in porous media, Phys. Rev. Fluids **2**, 103902 (2017).
[38] E. Lajeunesse, J. Martin, N. Rakotomalala, and D. Salin, 3D Instability of Miscible Displacements in a Hele-Shaw Cell, Phys. Rev. Lett. **79**, 5254 (1997).
[39] E. Lajeunesse, J. Martin, N. Rakotomalala, D. Salin, and Y. C. Yortsos, Miscible displacement in a Hele-Shaw cell at high rates, J. Fluid Mech. **398**, 299 (1999).
[40] I. Bischofberger, R. Ramachandran, and S. R. Nagel, Fingering versus stability in the limit of zero interfacial tension, Nat. Commun. **5**, 5265 (2014).
[41] I. Bischofberger, R. Ramachandran, and S. R. Nagel, An island of stability in a sea of fingers: emergent global features of the viscous-flow instability, Soft Matter **11**, 7428 (2015).

[42] R. J. Furbank and J. F. Morris, An experimental study of particle effects on drop formation, Phys. Fluids **16**, 1777 (2004).
[43] R. J. Furbank and J. F. Morris, Pendant drop thread dynamics of particle-laden liquids, Int. J. Multiphase Flow **33**, 448 (2007).
[44] C. Bonnoit, T. Bertrand, E. Clément, and A. Lindner, Accelerated drop detachment in granular suspensions, Phys. Fluids **24**, 043304 (2012).
[45] T. Bertrand, C. Bonnoit, E. Clément, and A. Lindner, Dynamics of drop formation in granular suspensions: the role of volume fraction, Granul. Matter **14**, 169 (2012).
[46] M. Z. Miskin and H. M. Jaeger, Droplet formation and scaling in dense suspensions, Proc. Natl. Acad. Sci. USA **109**, 4389 (2012).
[47] M. S. van Deen, T. Bertrand, N. Vu, D. Quéré, E. Clément, and A. Lindner, Particles accelerate the detachment of viscous liquids, Rheol. Acta **52**, 403 (2013).
[48] B. P. Cook, Theory for particle settling and shear-induced migration in thin-film liquid flow, Phys. Rev. E **78**, 045303 (2008).
[49] J. Zhou, B. Dupuy, A. L. Bertozzi, and A. E. Hosoi, Theory for Shock Dynamics in Particle-Laden Thin Films, Phys. Rev. Lett. **94**, 117803 (2005).
[50] T. Ward, C. Wey, R. Glidden, A. E. Hosoi, and A. L. Bertozzi, Theory for shock dynamics in particle-laden thin films, Phys. Fluids **21**, 083305 (2009).
[51] N. Murisic, J. Ho, V. Hu, P. Latterman, T. Koch, K. Lin, M. Mata, and A. L. Bertozzi, Particle-laden viscous thin-film flows on an incline: experiments compared with an equilibrium theory based on shear-induced migration and particle settling, Physica D **240**, 1661 (2011).
[52] N. Murisic, B. Pausader, D. Peschka, and A. L. Bertozzi, Dynamics of particle settling and resuspension in viscous liquid films, J. Fluid Mech. **717**, 203 (2013).
[53] A. Mavromoustaki and A. L. Bertozzi, Hyperbolic systems of conservation laws in gravity-driven, particle-laden thin-film flows, J. Eng. Math. **88**, 29 (2014).
[54] L. Wang and A. L. Bertozzi, Shock solutions for high concentration particle-laden thin films, SIAM J. Appl. Math. **74**, 322 (2014).
[55] S. Lee, Y. Stokes, and A. L. Bertozzi, Behavior of a particle-laden flow in a spiral channel, Phys. Fluids **26**, 043302 (2014).
[56] S. Lee, J. Wong, and A. L. Bertozzi, Equilibrium theory of bidensity particle-laden flows on an incline, in *Mathematical Modelling and Numerical Simulation of Oil Pollution Problems*, edited by M. Ehrhardt (Springer, New York, 2015).
[57] H. Tang, W. Grivas, D. Homentcovschi, J. Geer, and T. Singler, Stability Considerations Associated with the Meniscoid Particle Band at Advancing Interfaces in Hele-Shaw Suspension Flows, Phys. Rev. Lett. **85**, 2112 (2000).
[58] A. Ramachandran and D. T. Leighton, Particle migration in concentrated suspensions undergoing squeeze flow, J. Rheol. **54**, 563 (2010).
[59] F. Xu, J. Kim, and S. Lee, Particle-induced viscous fingering, J. Non-Newton. Fluid **238**, 92 (2016).
[60] J. Kim, F. Xu, and S. Lee, Formation and Destabilization of the Particle Band on the Fluid-Fluid Interface, Phys. Rev. Lett. **118**, 074501 (2017).
[61] C. Chevalier, A. Lindner, and E. Clement, Destabilization of a Saffman-Taylor Fingerlike Pattern in a Granular Suspension, Phys. Rev. Lett. **99**, 174501 (2007).
[62] Ø. Johnsen, C. Chevalier, A. Lindner, R. Toussaint, E. Clément, K. J. Måløy, E. G. Flekkøy, and J. Schmittbuhl, Decompaction and fluidization of a saturated and confined granular medium by injection of a viscous liquid or gas, Phys. Rev. E **78**, 051302 (2008).
[63] C. Chevalier, A. Lindner, M. Leroux, and E. Clément, Morphodynamics during air injection into a confined granular suspension, J. Non-Newton. Fluid **158**, 63 (2009).
[64] B. Sandnes, E. G. Flekkoy, H. A. Knudsen, K. J. Maloy, and H. See, Patterns and flow in frictional fluid dynamics, Nat. Commun. **2**, 288 (2011).
[65] J. A. Eriksen, B. Marks, B. Sandnes, and R. Toussaint, Bubbles breaking the wall: Two-dimensional stress and stability analysis, Phys. Rev. E **91**, 052204 (2015).

[66] C. E. Colosqui, J. F. Morris, and H. A. Stone, Hydrodynamically Driven Colloidal Assembly in Dip Coating, Phys. Rev. Lett. **110**, 188302 (2013).
[67] H. Thome, M. Rabaud, V. Hakim, and Y. Couder, The Saffman-Taylor instability: From the linear to the circular geometry, Phys. Fluids **1**, 224 (1988).
[68] J. F. Morris and F. Boulay, Curvilinear flows of noncolloidal suspensions: The role of normal stresses, J. Rheol. **43**, 1213 (1999).
[69] O. Giraldo, J. P. Durand, H. Ramanan, K. Laubernds, S. L. Suib, M. Tsapatsis, S. L. Brock, and M. Marquez, Dynamic organization of inorganic nanoparticles into periodic micrometer-scale patterns, Angew. Chem-Ger. Edit. **115**, 3011 (2003).
[70] M. Abkarian, J. Nunes, and H. A. Stone, Colloidal crystallization and banding in a cylindrical geometry, J. Am. Chem. Soc. **126**, 5978 (2004).
[71] M. Ghosh, F. Fan, and K. J. Stebe, Spontaneous pattern formation by dip coating of colloidal suspensions on homogeneous surfaces, Langmuir **23**, 2180 (2007).
[72] S. Watanabe, K. Inukai, S. Mizuta, and M. T. Miyahara, Mechanism for stripe pattern formation on hydrophilic surfaces by using convective self-assembly, Langmuir **25**, 7287 (2009).
[73] A Karnis and S. G. Mason, The flow of suspensions through tubes. VI. Meniscus effects, J. Colloid Interface Sci. **23**, 120 (1967).
[74] S. Bhattacharji and P. Savic, Real and apparent non-Newtonian behavior in viscous pipe flow of suspensions driven by a fluid piston, in *Proceedings of the 1965 Heat Transfer and Fluid Mechanics Institute*, edited by A. F. Charwat (Stanford University Press, Palo Alto, CA, 1965).
[75] C. W. Park and G. M. Homsy, Two-phase displacement in Hele Shaw cells: theory, J. Fluid Mech. **139**, 291 (1984).
[76] F. P. Bretherton, The motion of long bubbles in tubes, J. Fluid Mech. **10**, 166 (1961).
[77] D. Brutin, B. Sobac, and C. Nicloux, Influence of substrate nature on the evaporation of a sessile drop of blood, J. Heat Transfer **134**, 061101 (2012).
[78] R. D. Deegan, O. Bakajin, T. F. Dupont, G. Huber, S. R. Nagel, and T. A. Witten, Capillary flow as the cause of ring stains from dried liquid drops, Nature (London) **389**, 827 (1997).
[79] B. G. Prevo and O. D. Velev, Controlled, rapid deposition of structured coatings from micro- and nanoparticle suspensions, Langmuir **20**, 2099 (2004).
[80] T. Kraus, L. Malaquin, H. Schmid, W. Riess, N. D. Spencer, and H. Wolf, Nanoparticle printing with single-particle resolution, Nat. Nanotechnol. **2**, 570 (2007).